Molecular Therapy
Oncology
Original Article

Prognostic insights, immune infiltration, and therapeutic response: Cytoplasmic poly(A) tail regulators in hepatocellular carcinoma

Yi Liu,[1,5] Yan Huang,[2,5] Yunting Le,[1,5] Yating Gao,[1] Hui Wang,[1] Jing Yang,[1] Jialin Wang,[1] Chaoxia Zou,[1,3] and Qiang Li[4]

[1]Department of Biochemistry and Molecular Biology, Harbin Medical University, Harbin, Heilongjiang 150081, China; [2]Department of Neurobiology, Harbin Medical University, Harbin, Heilongjiang 150081, China; [3]Translational Medicine Research and Cooperation Center of Northern China, Heilongjiang Academy of Medicine Sciences, Harbin, Heilongjiang 150081, China; [4]Department of General Surgery, The Second Affiliated Hospital of Harbin Medical University, Harbin, Heilongjiang 150081, China

The presence of a poly(A) tail is indispensable for the post-transcriptional regulation of gene expression in cancer. This dynamic and modifiable feature of transcripts is under the control of various nuclear and cytoplasmic proteins. This study aimed to develop a novel cytoplasmic poly(A)-related signature for predicting prognosis, clinical attributes, tumor immune microenvironment (TIME), and treatment response in hepatocellular carcinoma (HCC). Utilizing RNA sequencing (RNA-seq) data from The Cancer Genome Atlas (TCGA), non-negative matrix factorization (NMF), and principal-component analysis (PCA) were employed to categorize HCC patients into three clusters, thus demonstrating the pivotal prognostic role of cytoplasmic poly(A) tail regulators. Furthermore, machine learning algorithms such as least absolute shrinkage and selection operator (LASSO), survival analysis, and Cox proportional hazards modeling were able to distinguish distinct cytoplasmic poly(A) subtypes. As a result, a 5-gene signature derived from TCGA was developed and validated using International Cancer Genome Consortium (ICGC) HCC datasets. This novel classification based on cytoplasmic poly(A) regulators has the potential to improve prognostic predictions and provide guidance for chemotherapy, immunotherapy, and transarterial chemoembolization (TACE) in HCC.

INTRODUCTION

Globally, hepatocellular carcinoma (HCC) accounted for 75%–85% of primary liver cancer cases and ranked sixth in cancer diagnoses and third in terms of cancer-related deaths, with approximately 906,000 new cases and 830,000 deaths in 2020.[1] A substantial proportion of HCC patients present with intermediate- or advanced-stage disease. For recurrent or advanced HCC, chemotherapy, immunotherapy, and transarterial chemoembolization (TACE) are preferred treatment options, but the overall survival of HCC patients remains poor.[2] In recent years, high-throughput sequencing has become popular and holds promise as a tool for predicting potential therapeutic targets in personalized medicine. Bioinformatics analysis of molecular mechanisms has emerged as a critical approach in cancer research.[3] Therefore, it is imperative to explore novel biomarkers in order to enhance prognostic predictive models for HCC.[4]

Polyadenylation is a critical post-transcriptional modification that occurs during mRNA processing in eukaryotic cells, involving the addition of an adenine nucleotide chain to the 3′ end of pre-mRNA molecules.[5] Various polyadenylation-regulating complexes and factors interact with the poly(A) tail of mRNA in the nucleus to ensure accurate cleavage and recognition of polyadenylation. Cytoplasmic polyadenylation determines the fate of RNA after export into the cytoplasm with the RNA-protein complex.[6] Since its discovery in sea urchin embryos in the 1970s, cytoplasmic polyadenylation has been observed in oocytes and early embryos across various animal species.[7–13] In somatic cells, elongation of poly(A) tails occurs in the cytoplasm, a process also demonstrated during neuronal plasticity and mitosis.[6,14] The dynamic and modifiable nature of the cytoplasmic poly(A) tail emphasizes the significance of sequences and proteins in regulating its length. Various sequence elements in the 3′ UTR, such as AU-rich elements, GU-rich elements, poly(A) limiting elements, and poly(A) signals, all play a role in influencing cytoplasmic poly(A) tail length through their interaction with poly(A)-binding proteins.[15] Furthermore, the presence of poly(A) tails in the cytoplasm can modulate translation efficiency during specific developmental stages by governing mRNA quality control and degradation.[16–18] In addition to impacting gamete development, inflammation, tumorigenesis and metastasis, obesity, synaptic plasticity, and long-term memory, post-transcriptional regulation of

Received 24 October 2023; accepted 19 May 2024;
https://doi.org/10.1016/j.omton.2024.200816.

[5]These authors contributed equally

Correspondence: Chaoxia Zou, Department of Biochemistry and Molecular Biology, Harbin Medical University, Harbin, Heilongjiang 150081, China.
E-mail: zouchaoxia006@hrbmu.edu.cn
Correspondence: Qiang Li, Department of General Surgery, The Second Affiliated Hospital of Harbin Medical University, Harbin, Heilongjiang 150081, China.
E-mail: lq_79224@163.com

cytoplasmic poly(A) tails influences a diverse array of biological processes.[19–23] However, there is currently limited understanding regarding the regulators of cytoplasmic poly(A) tails in HCC. Therefore, the objective of this study was to identify genes that regulate cytoplasmic poly(A) tails in HCC and establish a prognostic signature to gain insights into clinical outcomes, molecular mechanisms, and potential treatment strategies.

Numerous studies have investigated the correlation between biomarkers and HCC prognosis, yet the exploration of cytoplasmic poly(A) tail regulators as post-transcriptional modulators remains limited. The incorporation of cytoplasmic poly(A) tail-related signatures into prognostic models is seldom reported. A comprehensive analysis of cytoplasmic poly(A)-related cluster variations has been conducted using multi-omics analysis for both The Cancer Genome Atlas (TCGA) and independently validated International Cancer Genome Consortium (ICGC) cohorts, encompassing clinical relevance, survival analysis, and characterization of the tumor immune microenvironment. Furthermore, a nomogram was developed to predict the overall survival of HCC patients by integrating the prognostic signature of cytoplasmic poly(A) tail regulators with clinical data. Additionally, this study revealed an association between predicted risk and somatic mutations, tumor immune microenvironment traits, biological pathways, and HCC treatment options.

RESULTS

The landscape of cytoplasmic poly(A) tail regulators in HCC

The study collected a total of 24 genes involved in the regulation of cytoplasmic poly(A) tail mechanisms in eukaryotes. By analyzing the Cancer Genome Atlas Liver Hepatocellular Carcinoma (TCGA-LIHC) data on tumor and normal tissue expression profiles, we evaluated the differential expression profiling of these cytoplasmic poly(A) tail regulators in HCC. Our analysis revealed that most of these genes exhibited significantly higher levels in HCC compared to normal tissues, as demonstrated by a boxplot (Figure 1A). Furthermore, our investigation into copy number variation (CNV) showed that amplifications were more prevalent than deletions among the cytoplasmic poly(A) tail regulators (Figure 1B). In contrast, genetic mutations of cytoplasmic poly(A) tail regulators were infrequent in HCC (Figure 1C). Additionally, at the transcriptomic level, positive correlations were observed among cytoplasmic poly(A) tail regulators (Figure 1D). Moreover, our further analysis indicated frequent interactions among the cytoplasmic regulators of poly(A) tails (Figure 1E). Collectively, these findings suggest that cytoplasmic poly(A) tail regulators may play a significant role in modulating the progression of HCC.

Identification of cytoplasmic poly(A) tail-related HCC subgroups by the NMF method

Based on the analysis of differential expression profile of cytoplasmic poly(A) tail regulators in HCC, followed by identification of subgroups using non-negative matrix factorization (NMF), it is evident that cytoplasmic poly(A) tail regulators play a significant role in modulating HCC progression and are associated with distinct prognostic outcomes. We conducted an analysis of 24 cytoplasmic poly(A) tail regulators using a univariate Cox regression model. NMF clustering was applied to the TCGA-LIHC cohort, and the optimal number of clusters (K = 3) was determined based on optimal cophenetic coefficients from the "NMF" R package (Figures 2A and 2B). Three-dimensional principal-component analysis (3D-PCA) visually demonstrated distinct transcriptomic subgroups among the three clusters (Figure 2C). Notably, HCC patients in cluster 2 exhibited favorable overall survival compared to those in clusters 1 and 3, which had a poor prognosis (Figure 2D). Furthermore, noticeable differences were observed in the distribution of the cytoplasmic poly(A) tail regulator transcriptomic heatmaps among these three clusters (Figure 2E). Additionally, there were variations in clinical information across different clusters as well (Figure 2F).

Correlation between cytoplasmic poly(A) tail-related subgroups and TIME

After identifying distinct subgroups of HCC based on cytoplasmic poly(A) tail-related analysis using NMF, we examined the correlations between these subgroups and the tumor immune microenvironment (TIME), shedding light on potential impacts on immune regulation and mutational patterns. To gain an overview of the molecular mechanisms in the TCGA cohort, gene set variation analysis (GSVA) was performed to explore biological processes across the three clusters (Figure S1A). These results revealed strong activation of cell metabolism pathways such as fatty acid metabolism, xenobiotic metabolism, bile acid metabolism, adipogenesis, and peroxisomes in cluster 2, suggesting that cytoplasmic poly(A) tail regulators influence tumor cell metabolism. In contrast, clusters 1 and 3 showed inactivation of these metabolic pathways. Additionally, immune cell subpopulation correlations among the three clusters were assessed using boxplots generated by the CIBERSORT algorithm (Figure S1B). The findings demonstrated suppressed levels of monocytes, M1 macrophages, and M2 macrophages in clusters 1 and 3 compared to enhanced regulatory T cells, M0 macrophages, and follicular helper T cells. Waterfall plots showed that cluster 1 had the highest mutation rates in 10 genes: TP53 (30%), TTN (18%), CTNNB1 (15%), MUC16 (15%), AXIN1 (12%), CSMD3 (12%), PCLO (12%), ABCA13 (11%), ARID1A (11%), and SPTA1 (11%). In contrast, cluster 3 displayed the highest rates in 10 genes: TP53 (45%), TTN (25%), CTNNB1 (24%), MUC16 (20%), ALB (16%), CUBN (11%), MUC17 (11%), OBSCN (11%), PCLO (11%), and RYR2 (11%). Cluster 2 exhibited the highest rates in another 10 genes: CTNNB1 (32%), TTN (24%), TP53 (21%), MUC16 (15%), ALB (13%), APOB (11%), PCLO (10%), PRKDC (9%), LRP1B (9%), and OBSCN (9%) (Figures S1C–S1E). Clusters 1 and 3 exhibit similar immune-related mutation patterns. These clusters also appear more mutationally active in certain immune-related genes vs. cluster 2.

To further validate the similarity of clusters 1 and 3, we performed GSVA to assess differential gene set expression across three groups: cluster 1 vs. cluster 2, cluster 1 vs. cluster 3, and cluster

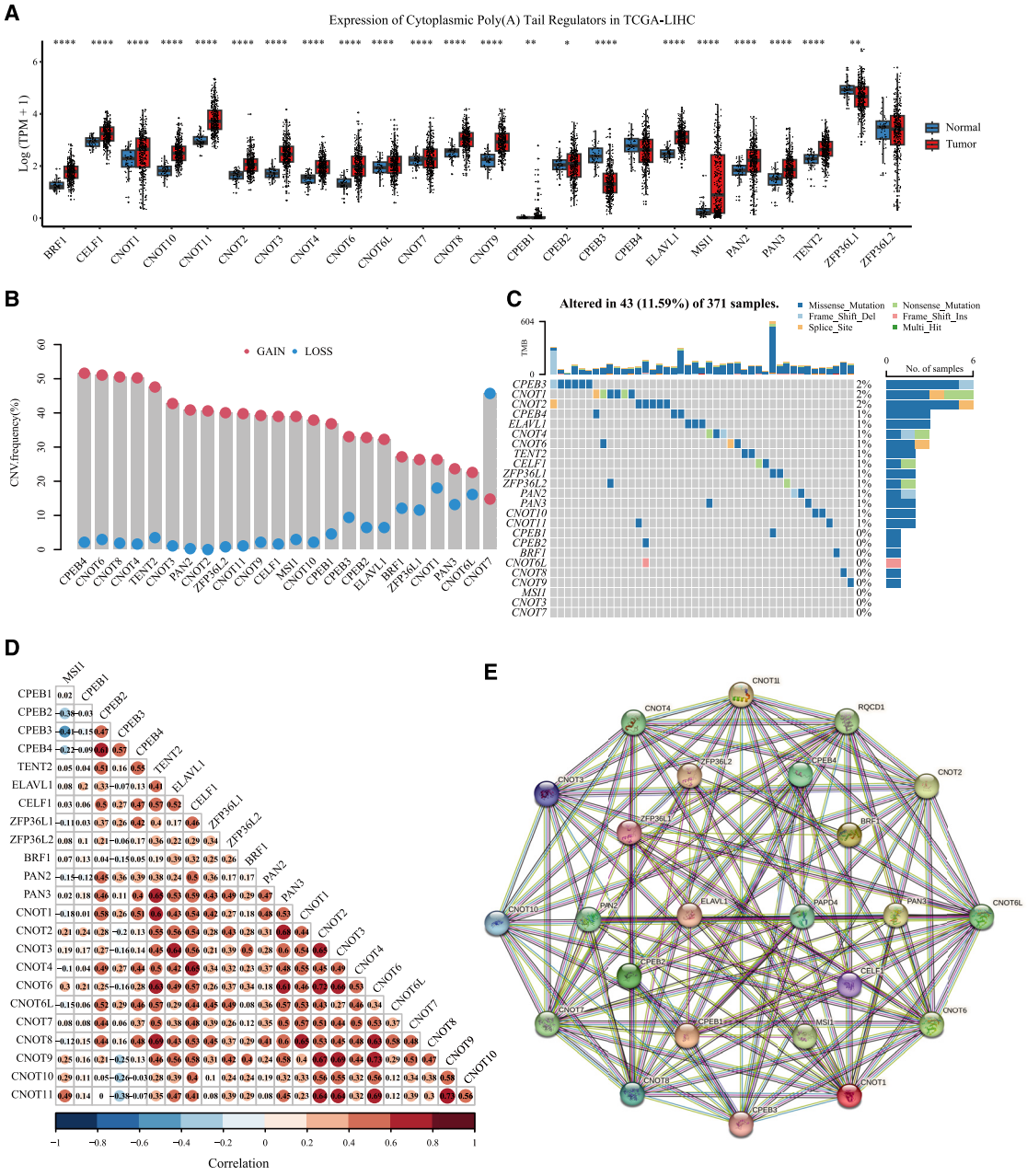

Figure 1. The landscape of cytoplasmic poly(A) tail regulators in HCC

(A) Differential expression profiling of cytoplasmic poly(A) tail regulators in HCC between tumor (n = 374) and normal (n = 50) tissue samples. (B) The CNV mutation frequency of cytoplasmic poly(A) tail regulators in the TCGA-LIHC cohort. The frequencies of copy number gain (red) and loss (blue) are shown. (C) Mutations of cytoplasmic poly(A) tail regulators were studied using the TCGA-LIHC cohort. Each sample is represented by a column, and each row corresponds to a specific cytoplasmic poly(A) tail regulator. The distinct mutations are indicated using different colors. (D) Correlations among cytoplasmic poly(A) tail regulators at the transcriptomic levels in HCC. (E) The PPI network of cytoplasmic poly(A) tail regulators.

2 vs. cluster 3 (Figures S2A–S2C). Subsequently, we conducted Gene Ontology (GO) enrichment analysis on the differentially expressed gene sets. The prominent shaded elements in Figure S2B suggest that there are no significant dissimilarities between clusters 1 and 3.

Generation of a cytoplasmic poly(A) tail regulator predictive signature in the TCGA-LIHC cohort

Investigation into the association between cytoplasmic poly(A) tail-related HCC subgroups and the tumor microenvironment provided valuable insights into immune regulation and mutational patterns,

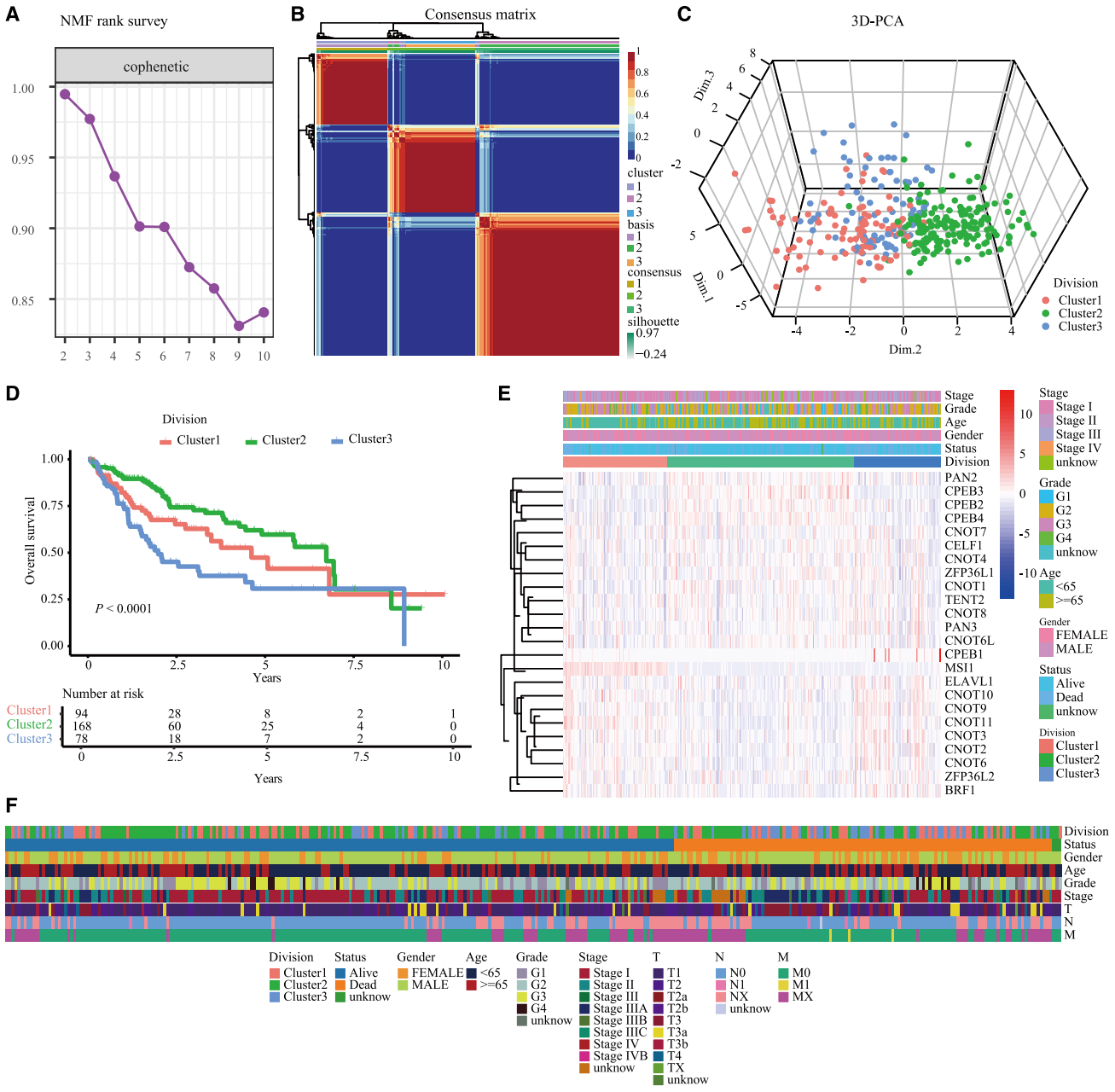

Figure 2. Identification of the cytoplasmic poly(A) tail-related subgroups of HCC by the NMF method

(A) Non-negative matrix factorization clustering of cytoplasmic poly(A) tail regulator-related subgroups in the TCGA-LIHC cohort. (B) Heatmap showing the consensus matrix of NMF clustering results using the gene expression data in the TCGA-LIHC cohort, colored by three HCC subgroups. (C) PCA among the three subgroups. (D) Kaplan-Meier survival analysis showed the different survival statuses among three HCC subgroups. (E) Transcription profile heatmap of cytoplasmic poly(A) tail regulators among three HCC subgroups. (F) Clinical information distribution of cytoplasmic poly(A) tail regulators in related subgroups.

leading to the development of a prognostic signature based on a subset of these cytoplasmic poly(A) tail regulators. To optimize the prognostic model's utility, least absolute shrinkage and selection operator (LASSO) logistic regression analysis identified five prognostic genes and their corresponding coefficients from 24 cytoplasmic poly(A) tail regulators (Figures 3A and 3B). The predictive model was constructed by incorporating the product of expression level and relative coefficient for each LASSO regression gene: risk score = (−0.3461481 × CPEB1 expression) + (−0.2409169 × CPEB3 expression) + (0.2658785 × CELF1 expression) + (0.3793337 × CNOT6 expression) + (0.1531105 × CNOT11 expression) (Figure 3E). Among 340 patients with complete clinical data, we

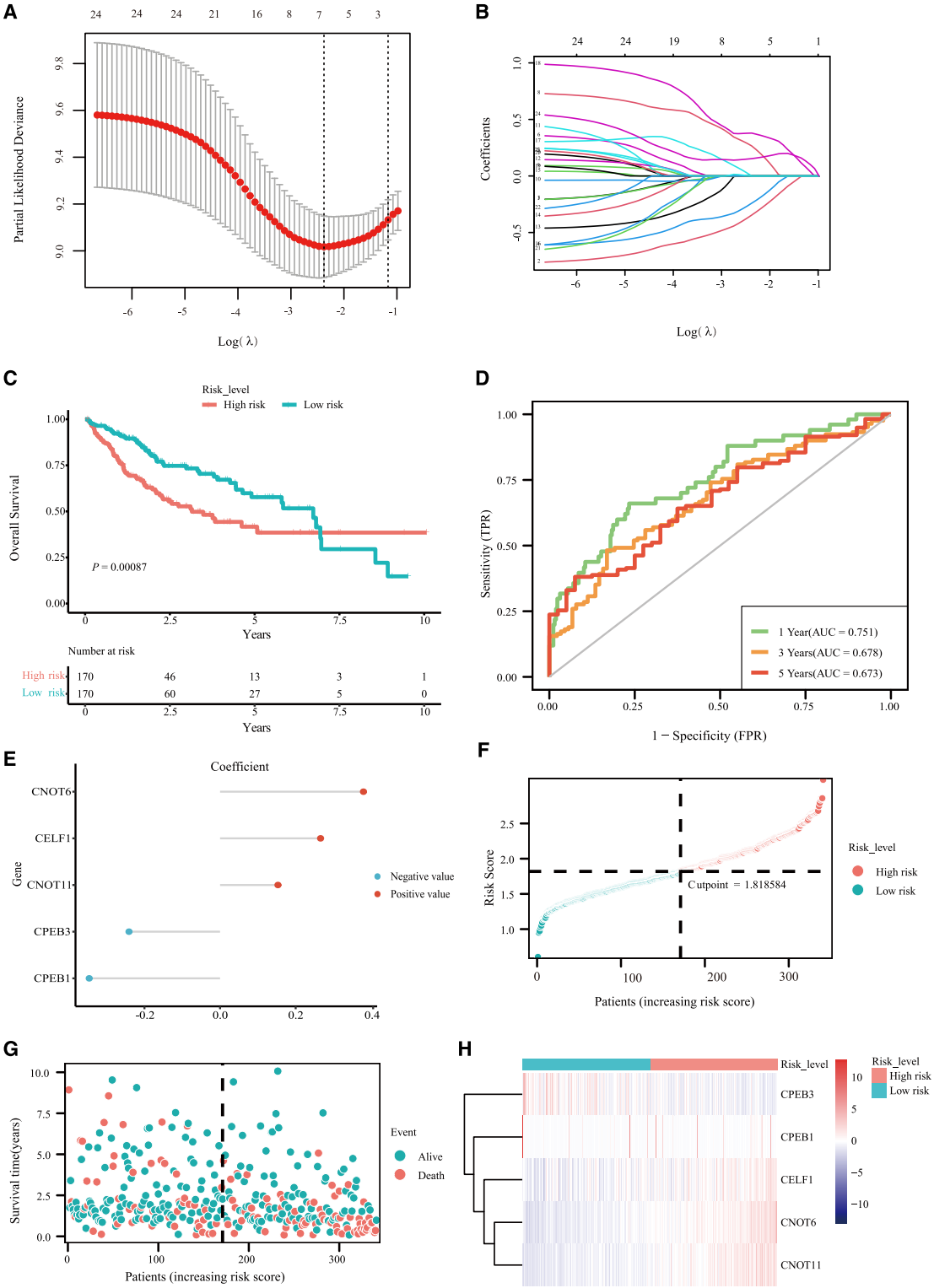

(legend on next page)

calculated the five-gene signature risk score and determined an optimal threshold value (cut point = 1.818584). Patients surpassing this threshold (n = 170) were classified as high-risk individuals, while those below it (n = 170) were categorized as low-risk individuals. Compared to the low-risk group, the high-risk group exhibited significantly shorter overall survival rates (Figure 3C). Time-dependent receiver operating characteristic (ROC) curves were employed to evaluate the accuracy of risk scores in predicting overall survival outcomes. The area under the curve (AUC) values at the 1-, 3-, and 5-year time points were found to be excellent at 0.751, 0.678, and 0.673, respectively, indicating strong predictive ability for prognosis assessment (Figure 3D). Elevated risk scores and death events were observed in HCC patients (Figures 3F and 3G). Notably, CNOT6, CELF1, and CNOT11 demonstrated upregulated expression, whereas CPEB3 displayed a negative correlation with risk scores. However, the heatmap representation of key genes did not clearly depict the expression pattern of CPEB1 (Figure 3H).

Formulation and assessment of a nomogram for predicting OS in the TCGA-LIHC cohort

Establishing a cytoplasmic poly(A) tail regulator prognostic signature provided valuable HCC prognosis insights and paved the way to formulate and assess a nomogram for predicting overall survival (OS) in the TCGA-LIHC cohort. The independence of the signature was assessed through univariate and multivariate Cox regression analyses. After adjusting for clinical parameters, the risk score retained robust prognostic capability for predicting OS (Figure 4C). An all-encompassing nomogram was formulated, incorporating all clinicopathological parameters (Figure 4A). Time-dependent ROC curve AUC analysis revealed that the nomogram exhibited superior prognostic capacity compared to using only the risk score alone (Figure 4B), highlighting its enhanced diagnostic precision. Calibration curves showed excellent performance of the nomogram when compared to an ideal model (Figure 4D). The nomogram facilitated more accurate prediction of 1-, 3-, and 5-year OS, yielding greater net benefits across most threshold probabilities (Figure 4E).

Validation of a cytoplasmic poly(A) tail regulator predictive signature in the ICGC LIRI-JP cohort

To validate the predictive accuracy of our model, we performed an analysis on an independent cohort of HCC patients from the International Cancer Genome Consortium Liver Cancer in Japan (ICGC LIRI-JP) dataset (n = 232). Employing the same cutoff value (1.818584), patients were stratified into high-risk (n = 108) and low-risk (n = 124) groups. Kaplan-Meier analysis revealed a significantly shorter OS in the high-risk group compared with the low-risk group (Figure S3A). Time-dependent ROC curves exhibited AUC values of 0.704, 0.761, and 0.627 for predicting 1-, 3-, and 5-year outcomes, respectively (Figure S3B). Furthermore, elevated risk scores and death events were observed in HCC patients (Figures S3C and S3D). A heatmap was generated to visualize gene expression profiles along with their corresponding risk scores for all included patients (Figure S3E).

Correlation between the TIME and cytoplasmic poly(A) tail regulator predictive signature

In the TCGA cohort, the low- and high-risk patient distribution across the three clusters was examined, revealing a substantial low-risk proportion in cluster 2, while high-risk patients predominated in clusters 1 and 3. These high-risk patients displayed heightened cytoplasmic poly(A) tail regulator mRNA expression (Figure S4A). In both the TCGA and ICGC cohorts, most cytoplasmic poly(A) tail regulators were notably upregulated compared to low-risk patients, as demonstrated by a boxplot to illustrate the expression of each cytoplasmic poly(A) tail regulator (Figures S4B and S4C), emphasizing the importance of transcriptomic distinctions between different risk groups. To investigate differences in immune cell infiltration, the relationships between immune cell infiltration and different risk groups were assessed using single-sample gene set enrichment analysis (ssGSEA). CD8+ T cells exhibited a negative correlation with cytoplasmic poly(A) tail regulators, while CD4+ T cells showed a positive correlation (Figures S5A and S6A). Diminished monocytes, CD8+ T cells, and natural killer cells alongside increased CD4+ T cells and activated dendritic cells were observed in high-risk compared to low-risk patients in the TCGA cohort (Figure S5B). Similar results were obtained in the ICGC cohort using ssGSEA (Figure S6B). Analysis of immune checkpoint molecule expression across cohorts revealed statistically significant differential expression of CTLA4, NT5E, PDCD1, KLRC1, TIGIT, and VSIR between low- and high-risk groups in the TCGA cohort (Figure S5C), suggesting a potential mechanism for immune tolerance and evasion. However, no significant differences in immune checkpoint expression were observed in the ICGC cohort (Figure S6C).

Functional enrichment analysis of the DEGs between the low- and high-risk groups

To investigate gene function and pathway differences between the two risk model subgroups, the "edgeR" R package was utilized to extract differentially expressed genes (DEGs) based on criteria of false discovery rate (FDR) < 0.01 and $|\log2FoldChange| \geq 1$. A Venn diagram analysis revealed a total of 409 upregulated and downregulated genes shared by both databases (Figure 5A). Functional enrichment analysis using GO indicated involvement in processes such as cell division/proliferation, lipoprotein synthesis/metabolism, lipid metabolism, and oxidoreductase activity (Figure 5B). Additionally, Kyoto Encyclopedia of Genes and Genomes (KEGG) enrichment analysis suggested

Figure 3. Generation of a cytoplasmic poly(A) tail regulator predictive signature in the TCGA-LIHC cohort

(A) The partial likelihood deviation for the LASSO Cox regression analysis. (B) LASSO coefficient profile plots for each independent variable. (C) Kaplan-Meier survival analysis showed the different survival statuses between low- and high-risk groups. (D) ROC curves of the cytoplasmic poly(A) tail regulator risk score for risk prediction of 1-, 3- and 5-year OS. (E) Coefficients of 5 key cytoplasmic poly(A) tail regulators. (F) Risk score distribution. (G) Heatmap of survival status. (H) Expression profile heatmap of 5 key cytoplasmic poly(A) tail regulators.

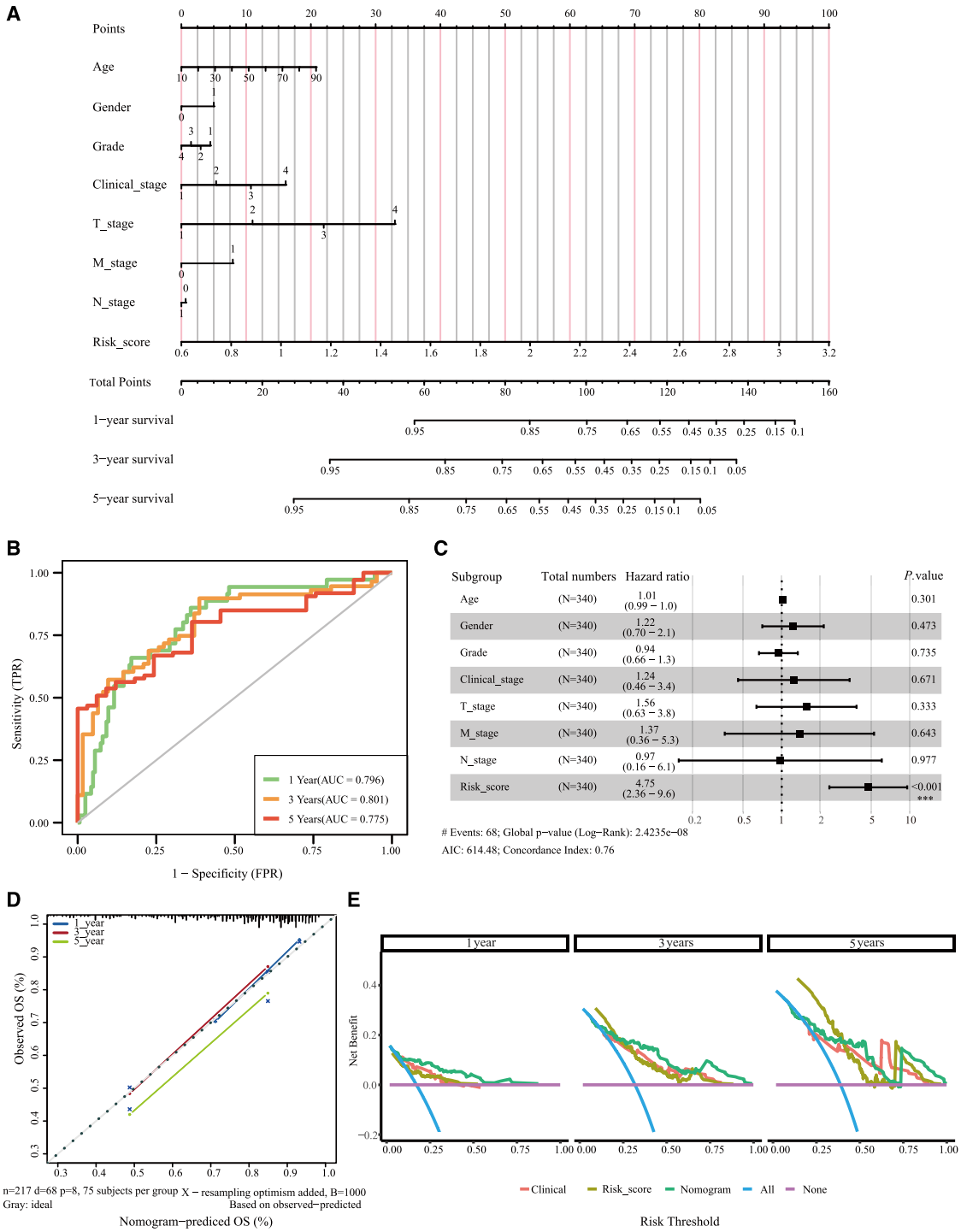

Figure 4. Formulation and assessment of a nomogram for predicting OS in the TCGA-LIHC cohort

(A) Generation of a nomogram combining the cytoplasmic poly(A) tail regulator risk score with other independent clinicopathological factors. (B) ROC curves of the nomogram for risk prediction. (C) Univariate and multivariate Cox regression analyses of the cytoplasmic poly(A) tail regulator risk score and clinicopathological parameters. (D) Calibration curves were generated to compare predicted survival probabilities from the nomogram with actual observed survival outcomes. On the x axis, the predicted survival probabilities from the nomogram are shown, while the y axis represents the corresponding actual survival probabilities. The diagonal reference line serves as a benchmark, representing the outcomes of a perfectly accurate predictive model. (E) Decision curve analysis of survival benefits corresponding to 1, 3, and 5 years.

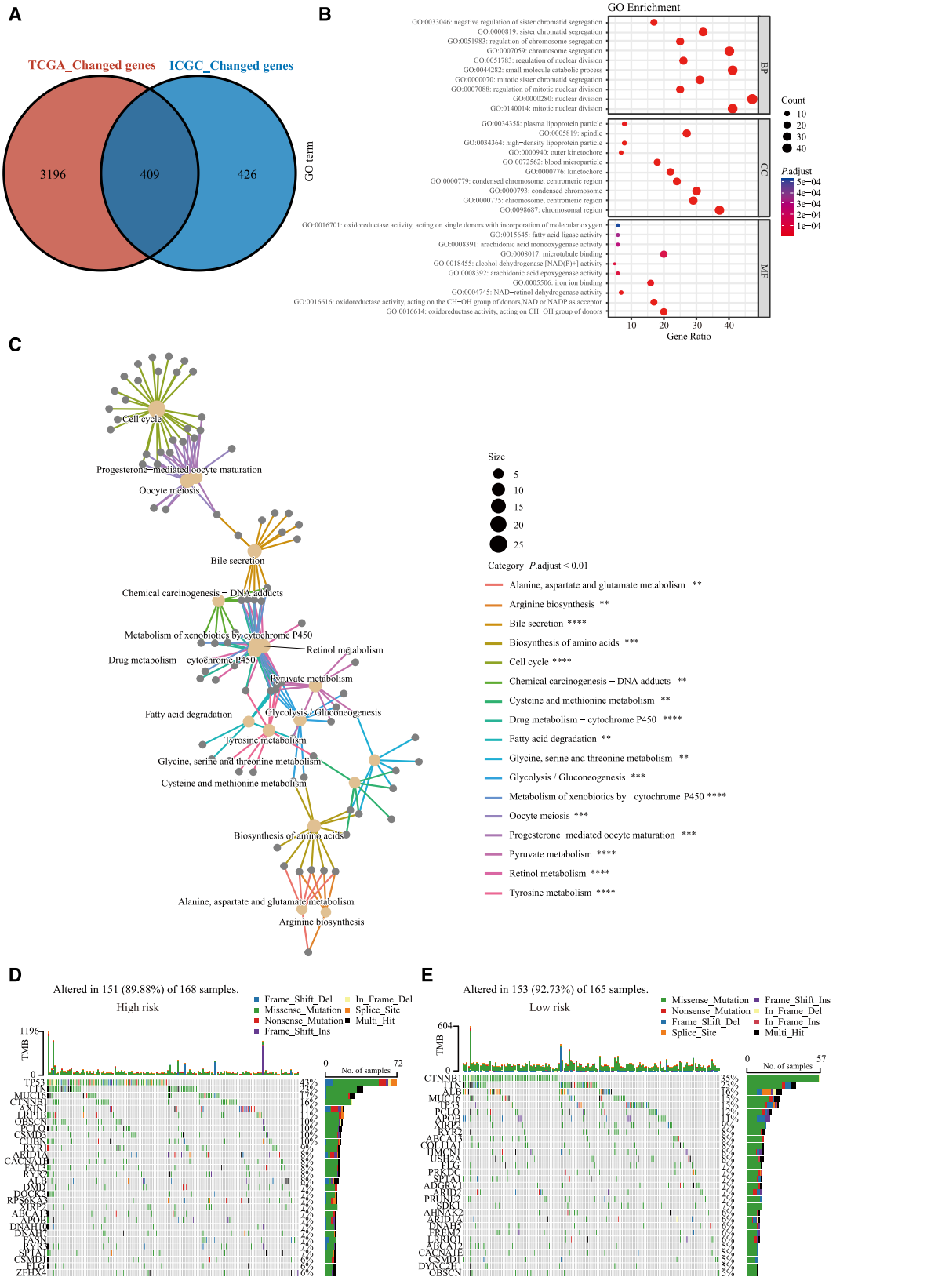

(legend on next page)

pathways including cell cycle, bile secretion, as well as glycolysis/amino acid metabolism (Figure 5C). Notably, TP53 (43%), TTN (23%), MUC16 (17%), CTNNB1 (16%), and AXIN1 (11%) were found to be the top 5 mutated genes in the high-risk group (Figure 5D), while CTNNB1 (35%), TTN (23%), ALB (16%), MUC16 (15%), and PCLO (15%) were observed as the top five mutated genes in the low-risk group (Figure 5E). These findings suggest a higher prevalence of immune-related mutations within the high-risk group, aligning with cluster 1/3 characteristics.

Relationship between the cytoplasmic poly(A) tail regulator signature and drug sensitivity and mainstream therapies (TACE and sorafenib)

The relationships between the cytoplasmic poly(A) tail regulator signature and drug sensitivity/mainstream HCC therapies were investigated. The Genomics of Drug Sensitivity in Cancer (GDSC2) drug response dataset identified 63 potential compounds for low- and high-risk groups (Figure S7). Immunotherapy response across HCC was evaluated using tumor immune dysfunction and exclusion (TIDE) scores, revealing decreased scores in high-risk patients (Figure 6A). Conversely, low-risk patients exhibited elevated exclusion scores (Figure 6B), while high-risk patients showed greater dysfunction scores (Figure 6C). Age younger than 65 years and female gender were significantly associated with elevated risk scores (Figures 6D and 6E). Higher risk scores were also correlated with advanced pathological grade/stage (Figures 6F and 6G), suggesting their utility as indicators of HCC progression. Analysis of the GSE109211 dataset showed increased non-responsiveness in high-risk patients (Figures 6I and 6J). High-risk patients also displayed higher expression of the sorafenib targets FGFR1, BRAF, RAF1, FLT1, and PDGFRB compared to low-risk patients (Figure 6H). Investigation of TACE response using the GSE104580 dataset found no significant difference between low- and high-risk groups (Figures 6K–6L), indicating limited benefits from conventional therapies for high-risk HCC patients.

Correlation between cytoplasmic poly(A) tail regulators and biological function and KEGG pathway in HCC

GSVA was employed to investigate the variation in biological process/KEGG pathways between different risk groups. The low-risk group showed significant enrichment in pathways such as oxidative phosphorylation, cholesterol homeostasis, fatty acid metabolism, xenobiotic metabolism, bile acid metabolism, adipogenesis, and peroxisomes. On the other hand, the high-risk group displayed enrichment in carcinogenic pathways, including unfolded protein response, myelocytomatosis oncogene (MYC) targets, DNA repair, mTORC1 signaling, G2/M phase cell cycle checkpoints, and E2F targets (Figure S8A). Furthermore, various metabolic activities, including amino acid metabolism, lipid metabolism, carbohydrate metabolism, and nucleotide metabolism, were significantly inhibited in the high-risk group (Figure S8B), affecting processes like hormone/vitamin synthesis and drug/toxin metabolism. The results clearly demonstrate a distinct functional differentiation between the different risk groups.

Experimental verification of CNOT6 and its relationships with HCC cell migration and proliferation

Considering the highest coefficient obtained from the LASSO regression algorithm, CNOT6 was selected as a representative example to explore its effect on HCC progression *in vitro*. Initially, CNOT6 was silenced in HCC cells to assess the transfection efficiency. siCNOT6-1 or siCNOT6-2 was transfected into Huh7 and Hep-G2 cells, demonstrating that small interfering RNA (siRNA) was successfully introduced into HCC cells (Figure 7A). Among these, siCNOT6-2 exhibited superior knockdown efficiency compared to siCNOT6-1 and was chosen for phenotypic experiments. A wound healing assay showed that silencing CNOT6 enhanced the migration capacity of both Huh7 and Hep-G2 cells (Figure 7B). Additionally, a Cell Counting Kit-8 (CCK-8) assay demonstrated a significant increase in cell viability upon knocking down CNOT6 in Huh7 and Hep-G2 cells (Figure 7C). Further evidence supporting this observation was provided by the Transwell assay, which showed that siCNOT6 promoted migration of both Huh7 and Hep-G2 cells (Figure 7D).

DISCUSSION

Based on previous comprehensive reviews and experimental findings, 24 genes have been identified that modulate the length of cytoplasmic poly(A) tails through distinct biological pathways, thereby influencing the initiation and progression of human disease.[6,24,25] However, recent research has revealed a more intricate role: cytoplasmic poly(A)-binding proteins can stimulate tail removal, impacting stability and translation, which, in turn, influences tail length.[25] Early investigations indicate that most mRNAs subject to cytoplasmic polyadenylation in oocytes and early embryos are directly associated with meiotic or mitotic processes.[26–28] In neuronal cells, cytoplasmic polyadenylation-mediated translation regulation in dendrites is thought to play a role in synaptic remodeling.[29] Cytoplasmic polyadenylation has also been implicated in the regulation of senescence and tumorigenesis.[30] Furthermore, the regulation of poly(A) tail size in the liver during the circadian rhythm involves both transcriptional upregulation and other mechanisms,[31] indicating widespread cooperation among different poly(A) regulatory factors. The increasing interest of researchers in cytoplasmic polyadenylation prompted our study to shed light on the significance of cytoplasmic poly(A) tail regulators in HCC. By modulating the length, stability, and structure of the tail, these factors may regulate RNA molecule function and fate, representing a crucial mechanism in HCC progression. We developed a signature for cytoplasmic poly(A) tail regulators that reflects patient subgroups with different transcriptomic profiles of the cytoplasmic poly(A) tail regulator, which holds potential for improving HCC treatment and research.

Figure 5. Functional enrichment analysis of the DEGs between the low- and high-risk groups

(A) Venn diagram showing the intersection results of up-regulated and down-regulated DEGs in the two datasets. (B) GO analysis of DEGs. (C) KEGG enrichment analysis of DEGs. (D and E) Waterfall plots showing the most frequently mutated genes in low- and high-risk groups, respectively.

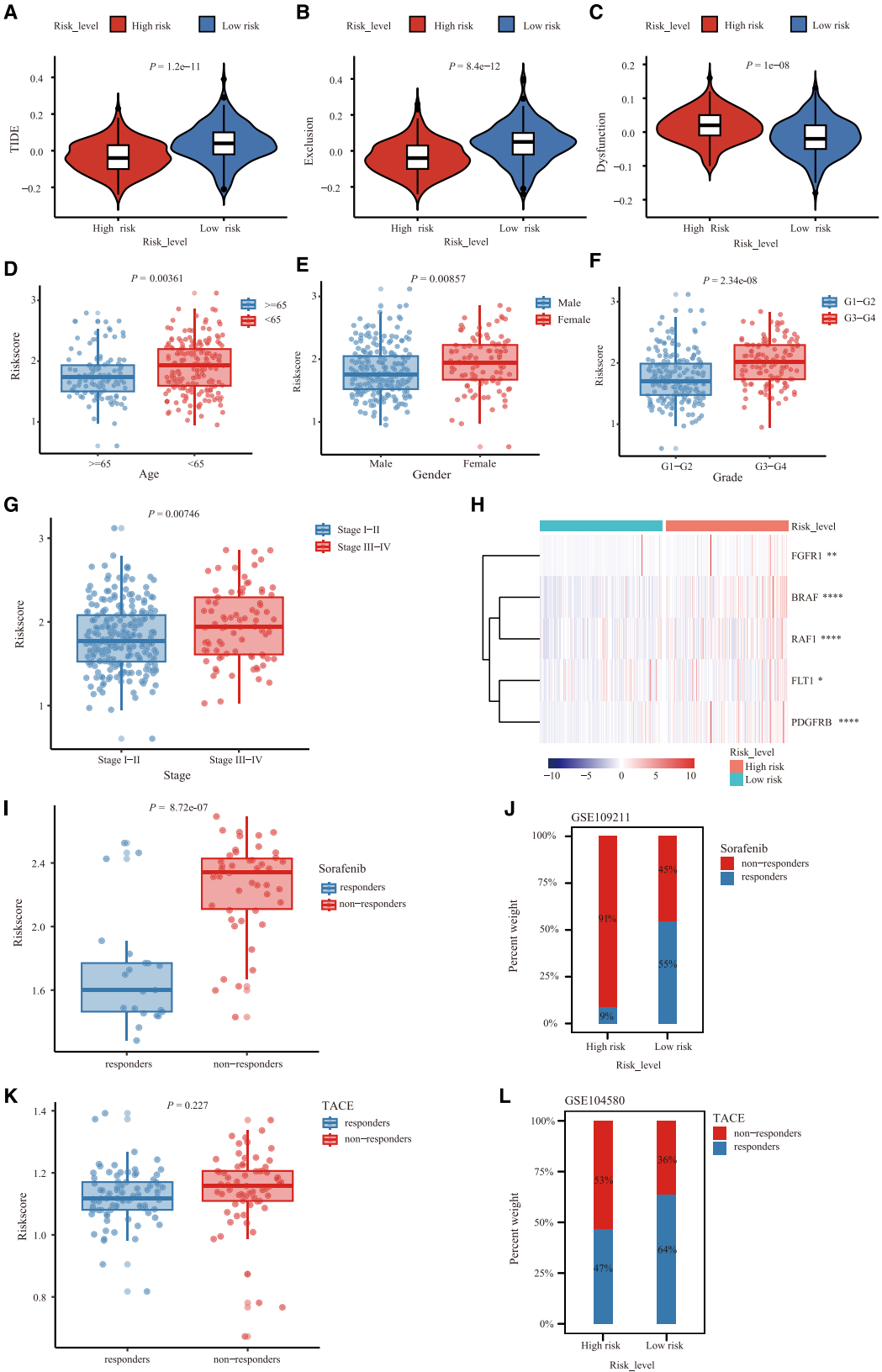

(legend on next page)

By analyzing the transcriptomic expression of 24 cytoplasmic poly(A) tail regulators in HCC tissues, NMF revealed the presence of three distinct subgroups. It was observed that clusters 1 and 3 were associated with a shorter OS compared to cluster 2. Furthermore, analysis of the TCGA cohort indicated that clusters 1 and 3 exhibited higher fractions of macrophages and Treg cells, which have previously been linked to poor OS in HCC.[32,33] LASSO analysis identified five prognostic genes (CPEB1, CPEB3, CELF1, CNOT6, and CNOT11) that regulate the poly(A) tail of mRNA in the cytoplasm. High-risk individuals exhibited significantly worse survival outcomes, establishing a link between the risk score and tumor progression. This finding was further validated in an independent ICGC LIRI-JP cohort. A nomogram integrating clinical data and risk score enabled optimized prediction of HCC. The identification of these five prognostic genes may represent important biomarkers for HCC. Specifically, CPEB1, a sequence-specific RNA-binding protein that regulates mRNA polyadenylation and translation, contributes to the suppression of cancer stemness in HCC.[34] In the same protein family as CPEB1, CPEB3 exerts inhibitory effects on hepatocarcinogenesis and tumor metastasis by modulating MTDH protein translation in HCC.[35] CELF1, also known as CUGBP1, exhibits high expression levels in the liver and governs the translation of proteins crucial for maintaining liver function.[36] Additionally, CNOT6, a component of the catalytic core of the CCR4-NOT transcriptional regulation complex, promotes mRNA decay of IRP1 in hepatoma carcinoma cells.[37] Furthermore, CNOT11, another constituent of the CCR4-NOT complex, initiates mRNA degradation by catalyzing poly(A) tail shortening in a process referred to as deadenylation.[38] In conclusion, all genes included in the prognostic model have been implicated previously in posttranscriptional modification. However, the specific role of these genes in influencing HCC patient prognosis through polyadenylation or deadenylation processes of certain genes remains to be elucidated, as there is limited research on how cytoplasmic polyadenylation-mediated regulation of gene poly(A) tail length impacts HCC occurrence and progression. It is noteworthy that knockdown of CNOT6 has been shown to accelerate HCC progression, which may seem contradictory to the positive coefficient obtained from LASSO regression analysis. Nevertheless, this result highlights the dual nature of CNOT6 as a potential biomarker for HCC. On one hand, its positive coefficient in LASSO regression reflects its upregulated expression in HCC tissue, suggesting that altered expression of CNOT6 may contribute to tumorigenesis.[39] On the other hand, the knockdown of CNOT6 leads to the destabilization of mRNA, which, in turn, may enhance the transcription of certain oncogenic genes through a mechanism of mRNA steady-state buffering in human HCC.[40] Intriguingly, while CNOT6 is highly expressed in HCC, its reduction can further propel cancer progression via this buffering mechanism. This dual role of CNOT6 in HCC highlights the complex interplay between gene expression and cancer progression, opening up numerous scientific inquiries for further investigation.

Compared to low-risk patients, high-risk patients demonstrate a modified distribution of immune cells, characterized by a decrease in monocytes, CD8+ T cells, and natural killer cells and an increase in CD4+ T cells and activated dendritic cell cells. This suggests the presence of a potential immune microenvironment conducive to disease progression or unfavorable clinical outcomes.[41] In high-risk patients, GSVA and GO analyses have revealed complex alterations in the regulation of biological processes. These changes encompass metabolic imbalance, aberrant immune responses, and abnormal cell growth cycles. Furthermore, KEGG pathway analysis identified alterations in metabolic pathways in high-risk patients. Various metabolism pathways, including one-carbon pool metabolism, amino acid metabolism, and lipid metabolism, were impacted. These changes are likely to affect hepatic metabolic regulation, encompassing lipid metabolism, amino acid metabolism, and antioxidant pathways. Additionally, the inhibition of drug metabolism pathways indicates a potential decrease in drug metabolism capability. Taken together, these findings suggest an aberrant state of hepatic cell metabolism in high-risk patients with implications for the onset and progression of liver cancer.[42]

Immune checkpoint inhibitors (ICIs), chemotherapy, TACE, and sorafenib are conventional clinical strategies for managing HCC.[43] This study confirmed the drug sensitivity of 63 compounds with a significance of $p < 0.0001$. These findings suggest that the risk score of cytoplasmic poly(A) tail regulators serves as a crucial biomarker for assessing immune status. Additionally, our investigation extended to explore the therapeutic response rate of ICIs based on the TIDE score. The high-risk group demonstrated a lower TIDE score, indicating potentially heightened responsiveness to ICI treatment. The aforementioned observations implied that patients in the high-risk group may display reduced sensitivity to sorafenib treatment. Consequently, we proposed a risk score with significant implications for chemotherapy, immunotherapy, and sorafenib treatment for HCC.

In conclusion, our study introduced a novel prognostic model based on cytoplasmic poly(A) tail regulators. This model demonstrated independent correlation with OS in both derivation and validation cohorts, providing insights into HCC prognosis, TIME, and potential therapeutic strategies.

Limitations of the study

While the ICGC validation cohort was incorporated into our research, it is important to acknowledge that public datasets may introduce bias

Figure 6. Relationship between the cytoplasmic poly(A) tail regulator signature and therapeutic response

(A) Difference in the TIDE score between the low- and high-risk groups. (B) Difference in the exclusion score between the high- and low-risk groups. (C) Difference in the dysfunction score between the high- and low-risk groups. (D–G) Comparison of the risk score between subgroup patients stratified by age (D), gender (E), grade (F), and stage (G). (H) Heatmap of the expression of several sorafenib targets in the low- and high-risk groups. (H and I) Difference in the risk score between sorafenib responders and non-responders in the GSE109211 cohort. (K and L) Difference in the risk score between TACE responders and non-responders in the GSE104580 cohort.

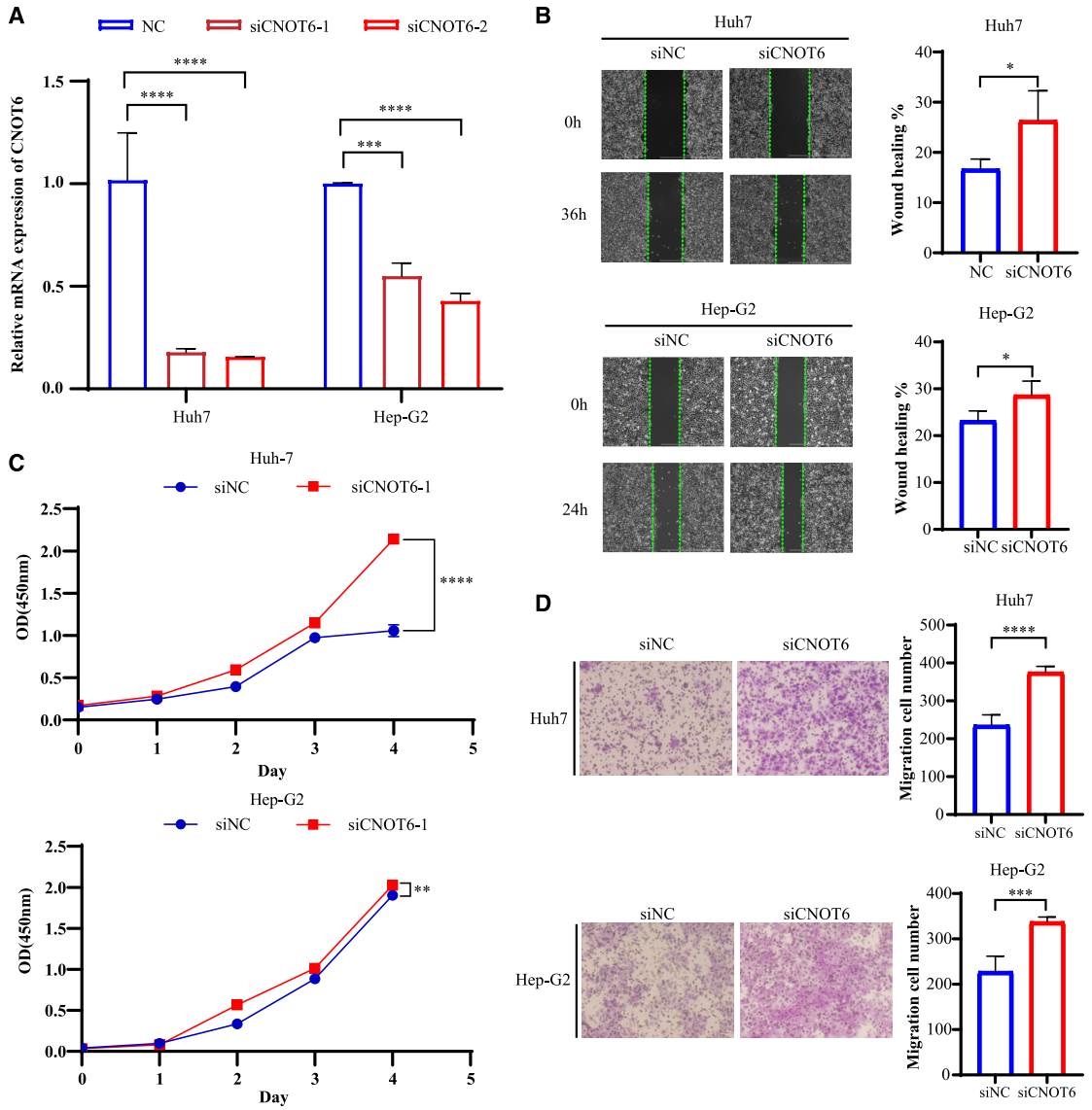

Figure 7. Experimental verification of CNOT6 and its relationships with HCC cell migration and proliferation

(A) The expression of CNOT6 after transfection of small interfering Negative Control (siNC), siCNOT6-1 or siCNOT6-2 in Huh7 and Hep-G2 cells was detected via RT-PCR. (B) The migration of Huh7 and Hep-G2 cells after transfection of siNC or siCNOT6-2 was calculated through a wound healing assay. Scale bar, 1,000 μm. (C) The viability of Huh7 and Hep-G2 cells after transfection of siNC or siCNOT6-2 was assessed by CCK-8 assay. (D) Transwell of Huh7 and Hep-G2 cells after transfection of siNC or siCNOT6-2. Scale bar, 64 μm.

that could potentially impact our findings. The underexplored areas of differential sorafenib/ICI response, immunological profile, and metabolic dysfunction by cytoplasmic poly(A) tail regulators warrant further investigation in future studies. Larger prospective studies are necessary to better validate the association between cytoplasmic poly(A) tail regulators, prognosis, and therapies. Currently, gene expression assessment relies on 5 cytoplasmic poly(A) tail regulators as a cost-effective alternative to full sequencing. The contribution of cytoplasmic poly(A) tail regulation to liver cancer development remains unclear and requires additional investigation.

MATERIALS AND METHODS

Patient cohort for multiple analyses

From the TCGA database (https://portal.gdc.cancer.gov/), transcriptional RNA sequencing, CNV, somatic mutation, and clinical data were obtained for the TCGA-LIHC cohort. The RNA sequencing panel included 374 HCC tumor tissues. Transcripts per kilobase million (TPM) and fragments per kilobase of transcript per million mapped reads (FPKM) values were utilized. TPM values were available for 374 HCC and 50 normal samples for analysis. A total of 371 samples from the TCGA were analyzed

for somatic mutations. Complete clinical data and cytoplasmic poly(A) tail regulator transcriptomic profiles were available for 340 patients. Raw read counts from the ICGC database (https://dcc.icgc.org/releases/current/Projects/LIRI-JP) were converted to comparable FPKM values. All 232 HCC samples with clinical data and RNA sequencing from ICGC were downloaded as an external validation set. Differential expression analysis of cytoplasmic poly(A) tail regulators was performed between tumors and paired normal tissues, gene CNV and somatic mutation landscapes were analyzed, and Pearson correlation analysis of cytoplasmic poly(A) tail regulator expression was conducted. Cytoplasmic poly(A) tail regulators were uploaded to the Search Tool for the Retrieval of Interacting Genes/Proteins (STRING) database (https://string-db.org/)[44] to generate a protein-protein interaction (PPI) network.

NMF classification of cytoplasmic poly(A) tail regulator subgroups

An NMF package called "NMF" was used to investigate unique cytoplasmic poly(A) tail-related subgroups.[45] This allowed decomposition of the original matrix into three non-negative matrices via the NMF algorithm, revealing potential gene expression profile characteristics. The number of clusters was set to range from 2 to 10. Optimal cluster number was determined by co-occurrence, dispersion, and contour indices as 3. The PCA scoring system based on the selected cytoplasmic poly(A) tail regulators was developed using the R package "FactoMineR." With the "survival" R package, OS for subtypes was analyzed, and Kaplan-Meier survival curves were plotted.

Estimation of TIME

To ensure reproducibility of the findings, three algorithms were utilized to estimate the TIME: Cell-type Identification by Estimating Relative Subsets of RNA Transcripts (CIBERSORT)[46] for estimating tumor-infiltrating immunological cell composition, ssGSEA[47] for estimating immune status, and TIDE[48] for predicting tumor cell escape capability.

Building and validating the cytoplasmic poly(A) regulator predictive signature

To further narrow down the candidate cytoplasmic poly(A) regulators, LASSO logistic regression and multivariate Cox regression models were utilized. This identified five key prognostic genes—CPEB3, CPEB1, CELF1, CNOT6, and CNOT11—based on minimum criteria. Using multivariate Cox regression coefficients, risk scores were computed by multiplying gene expression by a linear combination of the regression coefficients. Patients were assigned to high- and low-risk groups based on the median risk score. ROC curves and Kaplan-Meier analysis with the "timeROC" and "survival" R packages evaluated predictive reliability. To validate the signature in the ICGC cohort, identical analysis methods, risk score formula, and cutoff value were applied.

Establishment of a nomogram

Independent risk factors identified through multivariate Cox regression analysis were utilized to construct a nomogram for predicting OS probability with the "rms" R package.[49] The nomogram AUC was assessed using the "timeROC" package to determine reliability. Harrell's concordance index (C-index) quantified nomogram discrimination performance. The nomogram was validated with 1,000 bootstrap resamples to calculate a robust C-index, with 0.5 indicating random chance and 1.0 indicating maximum accuracy per ROC curve standards. Calibration curves evaluated calibration performance. Furthermore, decision curve analysis showed nomogram clinical utility and benefit at various threshold probabilities.[50]

Functional enrichment analysis

Gene sets for GSVA were obtained from the publicly accessible Molecular Signatures Database (https://www.gsea-msigdb.org/gse), including Hallmark (h.all.v2023.1.Hs.symbols), KEGG (c2.cp.kegg.v2023.1.Hs.symbols), and GO (c5.go.v2023.1.Hs.symbols) collections.[51] GSVA ascribed signaling pathway variation scores to gene sets, assessing biological significance.[52] TCGA-LIHC patients were divided into high- and low-risk groups based on the median risk score. DEG functional enrichment between groups was evaluated, with p values adjusted by Benjamini-Hochberg correction. DEGs were screened based on $|\log2FoldChange| \geq 1$ and FDR < 0.01 criteria. Additionally, DEGs underwent GO and (KEGG) enrichment analysis using the "clusterprofiler" R package[53] to identify enriched biological pathways and functions associated with cytoplasmic poly(A) tail regulators.

Therapeutic response analysis

The GSE104580[54] and GSE109211[55] datasets were utilized to analyze TACE and sorafenib sensitivity. Half-maximal inhibitory concentration values for 198 compounds were obtained from the GDSC2 database (https://www.cancerrxgene.org/). Subsequently, the "oncoPredict" R package determined compound sensitivity scores for individual high- and low-risk patients. Statistical significance was assessed by the Wilcoxon test at a significance threshold of $p < 0.0001$.

In vitro verification

The proliferation capability of HepG2 and Huh7 cells was estimated by using the CCK-8 assay (GlpBio, Montclair, CA, USA). The cells were inoculated in a 96-well plate (2×10^3/well) with 3 wells for each group. After silencing of CNOT6, the CCK-8 assay was performed by adding 10 μL of CCK-8 solution to each well, with subsequent incubation in an incubator for 2 h in a dark environment. Finally, the absorbance was analyzed at a 450-nm wavelength under a microplate reader (Tecan, Männedorf, Switzerland). A Transwell chamber (8-μm pore size, Corning, Corning NY, USA) was used. For the migration assay, cells (5.0×10^4 and 5.0×10^4 HepG2 and Huh7 cells, respectively) were suspended in 200 μL of fetal bovine serum (FBS)-free medium, and then the cells were pipetted into the upper chamber. At 48 h post-incubation at 37°C, methanol and

0.1% crystal violet were added to fix and stain the invaded cells in the lower chambers. A wound healing assay was used to assess the migration of HepG2 and Huh7 cells. After the cells formed a single cell layer, the cell monolayers were lightly scratched with the tip of a 200-μL pipette. Afterward, the cells were incubated in medium without FBS at 37°C for 24 h.

Statistical analysis

Statistical analyses for all bioinformatics were conducted using R software (v.4.2.1). The experimental data were analyzed and visualized using GraphPad Prism 9.5.1 software and statistically summarized with mean ± SD. Statistical analysis was performed using a Student's t test, with $p \leq 0.05$ considered statistically significant. ($^{*}p < 0.05$, $^{**}p < 0.01$, $^{***}p < 0.001$, $^{****}p < 0.0001$).

DATA AND CODE AVAILABILITY

The datasets presented in this study can be found in online repositories. The names of the repository/repositories and accession number(s) can be found in the article.

SUPPLEMENTAL INFORMATION

Supplemental information can be found online at https://doi.org/10.1016/j.omton.2024.200816.

ACKNOWLEDGMENTS

This work was supported by the National Natural Science Foundation of China (81572347). We deeply appreciate the data support from The Cancer Genome Atlas (TCGA), International Cancer Genome Consortium (ICGC), and Gene Expression Omnibus (GEO) data website.

AUTHOR CONTRIBUTIONS

All authors contributed significantly, and all authors are in agreement with the content of this manuscript. Y. Liu, Y.H., and Y. Le designed and implemented the research. Y. Liu, Y.H., Y. Le, Y.G., H.W., J.Y., and J.W. collated and analyzed the data. Y. Liu and Y.H. provided technical support. C.Z. and Q.L. provided language polishing for this article. Y. Liu wrote the manuscript. C.Z. revised the manuscript.

DECLARATION OF INTERESTS

The authors declare no competing interests.

REFERENCES

1. Sung, H., Ferlay, J., Siegel, R.L., Laversanne, M., Soerjomataram, I., Jemal, A., and Bray, F. (2021). Global Cancer Statistics 2020: GLOBOCAN Estimates of Incidence and Mortality Worldwide for 36 Cancers in 185 Countries. CA Cancer J. Clin. *71*, 209–249.
2. Yang, J.D., Hainaut, P., Gores, G.J., Amadou, A., Plymoth, A., and Roberts, L.R. (2019). A global view of hepatocellular carcinoma: trends, risk, prevention and management. Nat. Rev. Gastroenterol. Hepatol. *16*, 589–604.
3. Kyrochristos, I.D., Ziogas, D.E., and Roukos, D.H. (2019). Dynamic genome and transcriptional network-based biomarkers and drugs: precision in breast cancer therapy. Med. Res. Rev. *39*, 1205–1227.
4. Chen, S., Cao, Q., Wen, W., and Wang, H. (2019). Targeted therapy for hepatocellular carcinoma: Challenges and opportunities. Cancer Lett. *460*, 1–9.
5. Tian, B., Hu, J., Zhang, H., and Lutz, C.S. (2005). A large-scale analysis of mRNA polyadenylation of human and mouse genes. Nucleic Acids Res. *33*, 201–212.
6. Charlesworth, A., Meijer, H.A., and de Moor, C.H. (2013). Specificity factors in cytoplasmic polyadenylation. Wiley Interdiscip. Rev. RNA *4*, 437–461.
7. Wilt, F.H. (1973). Polyadenylation of maternal RNA of sea urchin eggs after fertilization. Proc. Natl. Acad. Sci. USA *70*, 2345–2349.
8. Fox, C.A., Sheets, M.D., and Wickens, M.P. (1989). Poly(A) addition during maturation of frog oocytes: distinct nuclear and cytoplasmic activities and regulation by the sequence UUUUUAU. Genes Dev. *3*, 2151–2162.
9. Standart, N., and Dale, M. (1993). Regulated polyadenylation of clam maternal mRNAs in vitro. Dev. Genet. *14*, 492–499.
10. Wang, L., Eckmann, C.R., Kadyk, L.C., Wickens, M., and Kimble, J. (2002). A regulatory cytoplasmic poly(A) polymerase in Caenorhabditis elegans. Nature *419*, 312–316.
11. Vassalli, J.D., Huarte, J., Belin, D., Gubler, P., Vassalli, A., O'Connell, M.L., Parton, L.A., Rickles, R.J., and Strickland, S. (1989). Regulated polyadenylation controls mRNA translation during meiotic maturation of mouse oocytes. Genes Dev. *3*, 2163–2171.
12. Suzuki, H., Tsukahara, T., and Inoue, K. (2009). Localization of c-mos mRNA around the animal pole in the zebrafish oocyte with Zor-1/Zorba. Biosci. Trends *3*, 96–104.
13. Paris, J., Osborne, H.B., Couturier, A., Le Guellec, R., and Philippe, M. (1988). Changes in the polyadenylation of specific stable RNA during the early development of Xenopus laevis. Gene *72*, 169–176.
14. Brawerman, G., and Diez, J. (1975). Metabolism of the polyadenylate sequence of nuclear RNA and messenger RNA in mammalian cells. Cell *5*, 271–280.
15. Jalkanen, A.L., Coleman, S.J., and Wilusz, J. (2014). Determinants and implications of mRNA poly(A) tail size–does this protein make my tail look big? Semin. Cell Dev. Biol. *34*, 24–32.
16. Subtelny, A.O., Eichhorn, S.W., Chen, G.R., Sive, H., and Bartel, D.P. (2014). Poly(A)-tail profiling reveals an embryonic switch in translational control. Nature *508*, 66–71.
17. Bresson, S.M., and Conrad, N.K. (2013). The human nuclear poly(a)-binding protein promotes RNA hyperadenylation and decay. PLoS Genet. *9*, e1003893.
18. Kumar, G.R., and Glaunsinger, B.A. (2010). Nuclear import of cytoplasmic poly(A) binding protein restricts gene expression via hyperadenylation and nuclear retention of mRNA. Mol. Cell Biol. *30*, 4996–5008.
19. Liu, Y., Zhao, H., Shao, F., Zhang, Y., Nie, H., Zhang, J., Li, C., Hou, Z., Chen, Z.J., Wang, J., et al. (2023). Remodeling of maternal mRNA through poly(A) tail orchestrates human oocyte-to-embryo transition. Nat. Struct. Mol. Biol. *30*, 200–215.
20. Kondrashov, A., Meijer, H.A., Barthet-Barateig, A., Parker, H.N., Khurshid, A., Tessier, S., Sicard, M., Knox, A.J., Pang, L., and De Moor, C.H. (2012). Inhibition of polyadenylation reduces inflammatory gene induction. RNA *18*, 2236–2250.
21. D'Ambrogio, A., Nagaoka, K., and Richter, J.D. (2013). Translational control of cell growth and malignancy by the CPEBs. Nat. Rev. Cancer *13*, 283–290.
22. Pell, N., Garcia-Pras, E., Gallego, J., Naranjo-Suarez, S., Balvey, A., Suñer, C., Fernandez-Alfara, M., Chanes, V., Carbo, J., Ramirez-Pedraza, M., et al. (2021). Targeting the cytoplasmic polyadenylation element-binding protein CPEB4 protects against diet-induced obesity and microbiome dysbiosis. Mol. Metab. *54*, 101388.
23. Eisen, T.J., Li, J.J., and Bartel, D.P. (2022). The interplay between translational efficiency, poly(A) tails, microRNAs, and neuronal activation. RNA *28*, 808–831.
24. Villalba, A., Coll, O., and Gebauer, F. (2011). Cytoplasmic polyadenylation and translational control. Curr. Opin. Genet. Dev. *21*, 452–457.
25. Passmore, L.A., and Coller, J. (2022). Roles of mRNA poly(A) tails in regulation of eukaryotic gene expression. Nat. Rev. Mol. Cell Biol. *23*, 93–106.
26. Piqué, M., López, J.M., Foissac, S., Guigó, R., and Méndez, R. (2008). A combinatorial code for CPE-mediated translational control. Cell *132*, 434–448.
27. Igea, A., and Méndez, R. (2010). Meiosis requires a translational positive loop where CPEB1 ensues its replacement by CPEB4. EMBO J. *29*, 2182–2193.
28. Mendez, R., Barnard, D., and Richter, J.D. (2002). Differential mRNA translation and meiotic progression require Cdc2-mediated CPEB destruction. EMBO J. *21*, 1833–1844.

29. Darnell, J.C., and Richter, J.D. (2012). Cytoplasmic RNA-binding proteins and the control of complex brain function. Cold Spring Harb. Perspect. Biol. *4*, a012344.

30. Fernández-Miranda, G., and Méndez, R. (2012). The CPEB-family of proteins, translational control in senescence and cancer. Ageing Res. Rev. *11*, 460–472.

31. Kojima, S., Sher-Chen, E.L., and Green, C.B. (2012). Circadian control of mRNA polyadenylation dynamics regulates rhythmic protein expression. Genes Dev. *26*, 2724–2736.

32. Zhou, S.L., Zhou, Z.J., Hu, Z.Q., Huang, X.W., Wang, Z., Chen, E.B., Fan, J., Cao, Y., Dai, Z., and Zhou, J. (2016). Tumor-Associated Neutrophils Recruit Macrophages and T-Regulatory Cells to Promote Progression of Hepatocellular Carcinoma and Resistance to Sorafenib. Gastroenterology *150*, 1646–1658.e17.

33. Zhang, Q., He, Y., Luo, N., Patel, S.J., Han, Y., Gao, R., Modak, M., Carotta, S., Haslinger, C., Kind, D., et al. (2019). Landscape and Dynamics of Single Immune Cells in Hepatocellular Carcinoma. Cell *179*, 829–845.e20.

34. Xu, M., Fang, S., Song, J., Chen, M., Zhang, Q., Weng, Q., Fan, X., Chen, W., Wu, X., Wu, F., et al. (2018). CPEB1 mediates hepatocellular carcinoma cancer stemness and chemoresistance. Cell Death Dis. *9*, 957.

35. Zhang, H., Zou, C., Qiu, Z., E, F., Li, Q., Chen, M., Wang, D., Tan, Q., Yin, W., Matunda, C., et al. (2020). CPEB3-mediated MTDH mRNA translational suppression restrains hepatocellular carcinoma progression. Cell Death Dis. *11*, 792.

36. Jones, K., Timchenko, L., and Timchenko, N.A. (2012). The role of CUGBP1 in age-dependent changes of liver functions. Ageing Res. Rev. *11*, 442–449.

37. Zhang, T., Sun, L., Hao, Y., Suo, C., Shen, S., Wei, H., Ma, W., Zhang, P., Wang, T., Gu, X., et al. (2022). ENO1 suppresses cancer cell ferroptosis by degrading the mRNA of iron regulatory protein 1. Nat. Cancer *3*, 75–89.

38. Raisch, T., and Valkov, E. (2022). Regulation of the multisubunit CCR4-NOT deadenylase in the initiation of mRNA degradation. Curr. Opin. Struct. Biol. *77*, 102460.

39. Song, P., Liu, S., Liu, D., Keijzers, G., Bakula, D., Duan, S., de Wind, N., Ye, Z., Vakhrushev, S.Y., Scheibye-Knudsen, M., et al. (2022). CNOT6: A Novel Regulator of DNA Mismatch Repair. Cells *11*, 521.

40. Singh, P., James, R.S., Mee, C.J., and Morozov, I.Y. (2019). mRNA levels are buffered upon knockdown of RNA decay and translation factors via adjustment of transcription rates in human HepG2 cells. RNA Biol. *16*, 1147–1155.

41. Fu, J., Xu, D., Liu, Z., Shi, M., Zhao, P., Fu, B., Zhang, Z., Yang, H., Zhang, H., Zhou, C., et al. (2007). Increased regulatory T cells correlate with CD8 T-cell impairment and poor survival in hepatocellular carcinoma patients. Gastroenterology *132*, 2328–2339.

42. Li, X., Ramadori, P., Pfister, D., Seehawer, M., Zender, L., and Heikenwalder, M. (2021). The immunological and metabolic landscape in primary and metastatic liver cancer. Nat. Rev. Cancer *21*, 541–557.

43. Kong, F.H., Ye, Q.F., Miao, X.Y., Liu, X., Huang, S.Q., Xiong, L., Wen, Y., and Zhang, Z.J. (2021). Current status of sorafenib nanoparticle delivery systems in the treatment of hepatocellular carcinoma. Theranostics *11*, 5464–5490.

44. Szklarczyk, D., Gable, A.L., Nastou, K.C., Lyon, D., Kirsch, R., Pyysalo, S., Doncheva, N.T., Legeay, M., Fang, T., Bork, P., et al. (2021). The STRING database in 2021: customizable protein-protein networks, and functional characterization of user-uploaded gene/measurement sets. Nucleic Acids Res. *49*. D605-d612.

45. Brunet, J.P., Tamayo, P., Golub, T.R., and Mesirov, J.P. (2004). Metagenes and molecular pattern discovery using matrix factorization. Proc. Natl. Acad. Sci. USA *101*, 4164–4169.

46. Newman, A.M., Liu, C.L., Green, M.R., Gentles, A.J., Feng, W., Xu, Y., Hoang, C.D., Diehn, M., and Alizadeh, A.A. (2015). Robust enumeration of cell subsets from tissue expression profiles. Nat. Methods *12*, 453–457.

47. Barbie, D.A., Tamayo, P., Boehm, J.S., Kim, S.Y., Moody, S.E., Dunn, I.F., Schinzel, A.C., Sandy, P., Meylan, E., Scholl, C., et al. (2009). Systematic RNA interference reveals that oncogenic KRAS-driven cancers require TBK1. Nature *462*, 108–112.

48. Jiang, P., Gu, S., Pan, D., Fu, J., Sahu, A., Hu, X., Li, Z., Traugh, N., Bu, X., Li, B., et al. (2018). Signatures of T cell dysfunction and exclusion predict cancer immunotherapy response. Nat. Med. *24*, 1550–1558.

49. Iasonos, A., Schrag, D., Raj, G.V., and Panageas, K.S. (2008). How to build and interpret a nomogram for cancer prognosis. J. Clin. Oncol. *26*, 1364–1370.

50. Vickers, A.J., and Elkin, E.B. (2006). Decision curve analysis: a novel method for evaluating prediction models. Med. Decis. Making *26*, 565–574.

51. Liberzon, A., Birger, C., Thorvaldsdóttir, H., Ghandi, M., Mesirov, J.P., and Tamayo, P. (2015). The Molecular Signatures Database (MSigDB) hallmark gene set collection. Cell Syst. *1*, 417–425.

52. Hänzelmann, S., Castelo, R., and Guinney, J. (2013). GSVA: gene set variation analysis for microarray and RNA-seq data. BMC Bioinf. *14*, 7.

53. Yu, G., Wang, L.G., Han, Y., and He, Q.Y. (2012). clusterProfiler: an R package for comparing biological themes among gene clusters. OMICS *16*, 284–287.

54. Ali, H.E.A., Emam, A.A., Zeeneldin, A.A., Srour, R., Tabashy, R., El-Desouky, E.D., Abd Elmageed, Z.Y., and Abdel-Wahab, A.H.A. (2019). Circulating miR-26a, miR-106b, miR-107 and miR-133b stratify hepatocellular carcinoma patients according to their response to transarterial chemoembolization. Clin. Biochem. *65*, 45–52.

55. Pinyol, R., Montal, R., Bassaganyas, L., Sia, D., Takayama, T., Chau, G.Y., Mazzaferro, V., Roayaie, S., Lee, H.C., Kokudo, N., et al. (2019). Molecular predictors of prevention of recurrence in HCC with sorafenib as adjuvant treatment and prognostic factors in the phase 3 STORM trial. Gut *68*, 1065–1075.